Dynamics and stability of Bose-Einstein condensates with attractive $1/r$ interaction

Holger Cartarius,* Tomaž Fabčič, Jörg Main, and Günter Wunner
Institut für Theoretische Physik 1, Universität Stuttgart, 70550 Stuttgart, Germany
(Received 12 March 2008; published 11 July 2008)

The time-dependent extended Gross-Pitaevskii equation for Bose-Einstein condensates with attractive $1/r$ interaction is investigated with both a variational approach and numerically exact calculations. We show that these condensates exhibit signatures known from the nonlinear dynamics of autonomous Hamiltonian systems. The two stationary solutions created in a tangent bifurcation at a critical value of the scattering length are identified as elliptical and hyperbolical fixed points, corresponding to stable and unstable stationary states of the condensate. The stable stationary state is surrounded by elliptical islands, corresponding to condensates periodically oscillating in time, whereas condensate wave functions in the unstable region undergo a collapse within finite time. For negative scattering lengths below the tangent bifurcation no stationary solutions exist, i.e., the condensate is always unstable and collapses.

DOI: 10.1103/PhysRevA.78.013615 PACS number(s): 03.75.Kk, 34.20.Cf, 04.40.−b, 05.45.−a

I. INTRODUCTION

Bose condensates with atomic interactions, in addition to the contact interaction, open the possibility to study the properties of degenerate quantum gases in which the relative strengths of long- and short-range interactions can be continuously adjusted by tuning the contact interaction via a Feshbach resonance. In particular, the Bose-Einstein condensation of neutral atoms with electromagnetically induced attractive $1/r$ interaction has been proposed. According to O'Dell *et al.* [1] "monopolar" quantum gases could be realized by a combination of six appropriately arranged "triads" of intense off-resonant laser beams. In that arrangement, the $1/r^3$ interactions of the retarded dipole-dipole interaction of neutral atoms in the presence of intense electromagnetic radiation are averaged out in the near-zone limit, while the weaker $1/r$ interaction is retained. An outstanding feature of this type of long-range interaction is that for attractive contact interaction stable Bose-Einstein condensates are predicted that are self-bound (without an additional trap). Despite the fact that a self-bound condensate with attractive $1/r$ interaction has not been realized in an experiment so far, the physical parameters necessary for creating it experimentally were discussed in detail by Giovanazzi *et al.* [2], who also obtained a theoretical prediction for the number of atoms in the self-bound condensate. Furthermore, the existence of stable monopole and quadrupole oscillations around the stationary ground state have been demonstrated and analyzed with analytical and numerical calculations [3].

The realization of self-bound condensates with attractive $1/r$ interaction in experiments remains a challenging task. However, experimental realization has been achieved for a similar system with a long-range interaction, viz. dipolar Bose-Einstein condensates. Here, the long-range dipole-dipole interaction appears next to the short-range contact term. The system has attracted much attention in recent years [4–8] and the achievement of Bose-Einstein condensation in a gas of chromium atoms [9], with a large dipole moment, has opened the way to promising experiments on dipolar quantum gases [10]. For example, the experimental observation of the dipolar collapse of a quantum gas has recently been reported by Koch *et al.* [11], which sets in when the contact interaction is reduced below some critical value.

Bose-Einstein condensates with attractive $1/r$ interaction exhibit a similar collapse scenario. Collapse of the self-bound condensates again only sets in below some critical value of the scattering length. It was recently shown [12] that these critical values in fact correspond to bifurcation points where two solutions of the Gross-Pitaevskii equation disappear: one the true ground state, the other a collectively excited state. It was also demonstrated [13] that at the bifurcation the two stationary solutions exhibit the typical structure known from studies of exceptional points [14–18] in open quantum systems described by non-Hermitian Hamiltonians. At the exceptional points both the energies and the corresponding wave functions are identical, a situation which is forbidden for bound states of the linear Schrödinger equation (which have to be orthogonal) but is possible here because of the nonlinearity of the Gross-Pitaevskii equation.

Using a complex continuation of the Gross-Pitaevskii equation the existence of complex eigenstates at (real) negative scattering lengths below the bifurcation point has also been revealed [13]. The physical interpretation of these states is the collapse (or explosion) of the condensate with a decay rate given by the imaginary part of the complex eigenvalues of the chemical potential.

It is the purpose of this paper to analyze self-bound spherically symmetric Bose condensates with attractive $1/r$ interaction in the vicinity of the bifurcation points from the point of view of nonlinear dynamics, and to investigate the time evolution of arbitrary condensate wave functions. We do this by solving the time-dependent Gross-Pitaevskii equation both by means of a variational approach with time-dependent Gaussian wave packets and by exact numerical computations using the split-operator method. We will show that of the two stationary solutions created in a tangent bifurcation one is dynamically stable and the other unstable, corresponding to elliptic and hyperbolic fixed points, respectively. The stable state is surrounded by solutions periodically oscillating in time, whereas wave functions in the un-

*Holger.Cartarius@itp1.uni-stuttgart.de

stable region undergo a collapse within finite time. Below the tangent bifurcation no stationary solutions exist, i.e., the condensate is always unstable and collapsing.

The special appeal of investigations of the properties of spherically symmetric self-trapped Bose condensates with attractive $1/r$ interaction lies in the fact that the extremization of the variational mean-field energy can be carried out fully analytically. The reason is that in absence of a trap the extremization conditions for the mean-field energy become quadratic equations, while with a trap potential the equations become at least polynomials of order 5, caused by the combination of the trap and contact interaction terms, regardless of whether or not a long-range interaction is present, and of its type. Therefore generic properties of Bose condensates can be elucidated in a very simple and transparent way, and later be checked in numerical calculations and in more complex systems such as dipolar Bose condensates.

The evolution of a wave function is determined by the extended Gross-Pitaevskii equation for self-trapped Bose-Einstein condensates with attractive $1/r$ interaction without external trap potential, which reads

$$i\frac{d}{dt}\psi(\boldsymbol{r},t) = \left(-\Delta + 8\pi Na|\psi(\boldsymbol{r},t)|^2 - 2N\int d^3\boldsymbol{r}'\frac{|\psi(\boldsymbol{r}',t)|^2}{|\boldsymbol{r}-\boldsymbol{r}'|}\right)\psi(\boldsymbol{r},t), \tag{1}$$

where the natural "atomic" units introduced in Ref. [12] were used. Lengths are measured in units of a "Bohr radius" $a_u = \hbar^2/(mu)$, energies in units of a "Rydberg energy" $E_u = \hbar^2/(2ma_u^2)$, and times in units of $t_u = \hbar/E_u$, where u determines the strength of the atom-atom interaction [1], and m is the mass of one boson. The number of bosons is N.

The paper is organized as follows. In Sec. II the basic equations resulting from a time-dependent variational principle applied to the Gross-Pitaevskii equation are presented, where the solution of the nonlinear partial differential equation is reduced to a set of ordinary first order differential equations. The linear stability of the fixed points is investigated with variational as well as numerically exact calculations in Sec. III. In Sec. IV the dynamics of the condensate obtained from variational and from numerically exact computations is investigated and the results are compared. Conclusions are drawn in Sec. V.

II. TIME-DEPENDENT VARIATIONAL PRINCIPLE

We apply the time-dependent variational principle (TDVP) [19,20] to solving the time-dependent Gross-Pitaevskii (GP) equation. Exploiting the scaling properties presented in Ref. [12] and introducing the scaled variables

$$(\tilde{\boldsymbol{r}},\tilde{a},\tilde{t},\tilde{\psi}) = (N\boldsymbol{r},N^2a,N^2t,N^{-3/2}\psi), \tag{2}$$

we bring the system in the form

$$i\frac{d}{d\tilde{t}}\tilde{\psi}(\tilde{\boldsymbol{r}},\tilde{t}) = \tilde{H}\tilde{\psi}(\tilde{\boldsymbol{r}},\tilde{t}) = [-\Delta_{\tilde{r}} + \tilde{V}_c + \tilde{V}_u]\tilde{\psi}(\tilde{\boldsymbol{r}},\tilde{t}), \tag{3}$$

where the potentials

$$\tilde{V}_c = 8\pi\tilde{a}|\tilde{\psi}(\tilde{\boldsymbol{r}},\tilde{t})|^2, \tag{4a}$$

$$\tilde{V}_u = -2\int d^3\tilde{\boldsymbol{r}}'\frac{|\tilde{\psi}(\tilde{\boldsymbol{r}}',\tilde{t})|^2}{|\tilde{\boldsymbol{r}}'-\tilde{\boldsymbol{r}}'|} \tag{4b}$$

depend on the coordinates and the wave function, i.e., $\tilde{H}$ is a nonlinear operator. The scaling reveals that the system has only one external parameter, viz., $\tilde{a}=N^2a/a_u$ [12]. If not stated otherwise, we use the scaled variables throughout the rest of the paper and omit the tilde in what follows.

An approximate solution $\psi(t)$ on a given manifold in Hilbert space is obtained by minimizing the quantity $I=\|i\dot{\phi}(t) - H\psi(t)\|^2$ with respect to ϕ only, and then setting $\dot{\psi}\equiv\phi$. This means that the time-dependent variational principle does not depend on properties of the operator H, i.e., the method can be applied to linear and nonlinear operators in the same way. Let the wave function be parametrized by a set of complex time-dependent functions $z(t)=\{z_1(t),\ldots,z_n(t)\}$, i.e., $\psi(t) = \psi[z(t)]$. The TDVP yields a set of ordinary differential equations for the motion of $z(t)$

$$K\dot{z} = -i\boldsymbol{h} \tag{5}$$

with the matrix K and the vector $\boldsymbol{h}$ of the n-dimensional system (5) given by

$$K = \left\langle \frac{\partial\psi}{\partial z}\middle|\frac{\partial\psi}{\partial z}\right\rangle, \quad \boldsymbol{h} = \left\langle \frac{\partial\psi}{\partial z}\middle|H\middle|\psi\right\rangle. \tag{6}$$

In time-independent calculations for condensates with $1/r$ interaction Gaussian wave functions have been used as an ansatz for the two solutions created in the tangent bifurcation [1,12]. To apply the TDVP to the Gross-Pitaevskii Eq. (1) we choose as a test function a radially symmetric Gaussian wave packet

$$\psi(r,t) = e^{i(Ar^2+\gamma)} = e^{-(A_ir^2+\gamma_i)+i(A_rr^2+\gamma_r)} \tag{7}$$

with the time-dependent variational parameters $z(t) = \{A(t),\gamma(t)\} = \{A_r(t)+iA_i(t),\gamma_r(t)+i\gamma_i(t)\}$. A similar time-dependent Gaussian trial function has been applied in studies of the dynamics of the Gross-Pitaevskii equation without $1/r$ interaction [21]. Evaluation of K and $\boldsymbol{h}$ in Eqs. (5) and (6) yields the ordinary differential equations

$$\dot{A} = -4A^2 - \frac{1}{2}V_2, \tag{8a}$$

$$\dot{\gamma} = 6iA - v_0, \tag{8b}$$

where v_0 and V_2 are given as solutions of the two linear equations

$$\langle\psi|\psi\rangle v_0 + \frac{1}{2}\langle\psi|r^2|\psi\rangle V_2 = \langle\psi|V_c+V_u|\psi\rangle, \tag{9a}$$

$$\langle\psi|r^2|\psi\rangle v_0 + \frac{1}{2}\langle\psi|r^4|\psi\rangle V_2 = \langle\psi|r^2(V_c+V_u)|\psi\rangle, \tag{9b}$$

with

$$\langle\psi|\psi\rangle = \frac{\pi^{3/2}}{2\sqrt{2}} e^{-2\gamma_i} A_i^{-3/2}, \tag{10a}$$

$$\langle\psi|r^2|\psi\rangle = \frac{3\pi^{3/2}}{8\sqrt{2}} e^{-2\gamma_i} A_i^{-5/2}, \tag{10b}$$

$$\langle\psi|r^4|\psi\rangle = \frac{15\pi^{3/2}}{32\sqrt{2}} e^{-2\gamma_i} A_i^{-7/2}, \tag{10c}$$

$$\langle\psi|V_c|\psi\rangle = \pi^{5/2} a e^{-4\gamma_i} A_i^{-3/2}, \tag{10d}$$

$$\langle\psi|V_u|\psi\rangle = -\frac{\pi^{5/2}}{2} e^{-4\gamma_i} A_i^{-5/2}, \tag{10e}$$

$$\langle\psi|r^2 V_c|\psi\rangle = \frac{3\pi^{5/2}}{8} a e^{-4\gamma_i} A_i^{-5/2}, \tag{10f}$$

$$\langle\psi|r^2 V_u|\psi\rangle = -\frac{5\pi^{5/2}}{16} e^{-4\gamma_i} A_i^{-7/2}. \tag{10g}$$

Inserting v_0 and V_2 in Eqs. (8a) and (8b) leads to the differential equations

$$\dot{A} = -4A^2 + 2\sqrt{2}\pi e^{-2\gamma_i}\left(aA_i - \frac{1}{6}\right), \tag{11a}$$

$$\dot{\gamma} = 6iA + \frac{\pi e^{-2\gamma_i}}{2\sqrt{2A_i}}(5 - 14aA_i). \tag{11b}$$

The imaginary part of Eq. (11b) can be integrated analytically

$$\gamma_i(t) = -\frac{3}{4}\ln\frac{2A_i(t)}{\pi} \tag{12}$$

and guarantees the normalization condition $\|\psi\|^2 = 1$. The final form of the equations of motion in real number representation is given by

$$\dot{A}_r = -4(A_r^2 - A_i^2) + \frac{8}{\sqrt{\pi}} A_i^{3/2}\left(aA_i - \frac{1}{6}\right), \tag{13a}$$

$$\dot{A}_i = -8A_r A_i, \tag{13b}$$

$$\dot{\gamma}_r = -6A_i + \frac{1}{\sqrt{\pi}}\sqrt{A_i}(5 - 14aA_i), \tag{13c}$$

which are solved under the initial conditions $A_r(0) = \gamma_r(0) = 0$, $A_i(0) > 0$ for an initially real valued Gaussian wave packet.

III. LINEAR STABILITY OF THE BIFURCATING STATES

In this section we study the stability of the two stationary eigenstates that are born in the tangent bifurcation. We do this first for the variational solutions, and then demonstrate how the essential features carry over to the analysis of the numerically exact solutions.

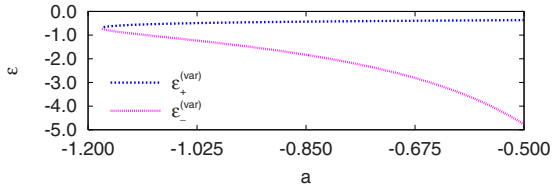

FIG. 1. (Color online) Chemical potentials of the ground state (ε_+) and the nodeless excited state (ε_-) in the variational calculation. They emerge in a tangent bifurcation at a critical value of the scaled scattering length $a_{cr} = -3\pi/8 = -1.1780$ [12].

A. Stability of the variational solutions

In the time-dependent variational approach, the two stationary states of the Gross-Pitaevskii Eq. (3) appear as the time-independent solutions (fixed points) of the equations of motion (13a)–(13c). Requiring $\dot{A}_i = 0$ and $\dot{A}_r = 0$ immediately leads to

$$\hat{A}_r = 0, \tag{14a}$$

$$\hat{A}_i = \frac{1}{6a} + \frac{\pi}{8a^2}\left(1 \pm \sqrt{1 + \frac{8a}{3\pi}}\right). \tag{14b}$$

The vanishing of the real part of $\hat{A}$ implies that the state indeed is a stationary Gaussian. The scaled chemical potentials ε are given by the negative time derivative $-\dot{\gamma}_r$ of the phase of the wave function in Eq. (13c)

$$\varepsilon_\pm^{(\mathrm{var})} = -\dot{\gamma}_r = -\frac{4}{9\pi}\frac{5 \pm 4\sqrt{1 + \frac{8a}{3\pi}}}{\left(1 \pm \sqrt{1 + \frac{8a}{3\pi}}\right)^2}. \tag{15}$$

The chemical potentials of the two solutions (15) are drawn in Fig. 1. The tangent bifurcation behavior of the chemical potential at the critical scattering length $a_{cr} = -3\pi/8 = -1.1780$ is clearly visible. The branch with the lower chemical potential in Fig. 1 turns out to have higher mean-field energy than the other branch. Therefore the plus sign refers to the ground state, and the minus sign to the collectively excited state.

The results obtained here via the fixed points of the time-dependent equations of motion for the variational parameters fully agree with the results derived in Refs. [1,12] applying a time-independent variational approach to extremize the mean-field energy, and which were used to compare with numerically exact solutions of the stationary extended Gross-Pitaevskii equation in Refs. [12,13]. The linearization of the equations of motion (13a)–(13c) around the stationary solutions $\hat{A}_r$, $\hat{A}_i$ are given by

$$\delta\dot{A}_{r\pm} = \pm\frac{8}{9\pi}\frac{\sqrt{1 + \frac{8a}{3\pi}}}{\left(\sqrt{1 + \frac{8a}{3\pi}} \pm 1\right)^2}\delta A_{i\pm}, \tag{16a}$$

$$\delta\dot{A}_{i\pm} = -\frac{32}{9\pi}\frac{1}{\left(\sqrt{1+\frac{8a}{3\pi}}\pm 1\right)^2}\delta A_{r\pm}. \tag{16b}$$

The eigenmodes with the eigenvalues $\lambda^{(\mathrm{var})}$ of Eqs. (16a) and (16b) are calculated with the usual ansatz $\delta A_{r,i}(t) = \delta A_{r,i}^{(0)} e^{\lambda^{(\mathrm{var})}t}$. For the stationary ground state we find the two eigenvalues

$$\lambda_{+}^{(\mathrm{var})} = \pm\frac{16i}{9\pi}\frac{\sqrt[4]{1+\frac{8a}{3\pi}}}{\left(\sqrt{1+\frac{8a}{3\pi}}+1\right)^2}, \tag{17}$$

which are always imaginary for $a > -3\pi/8$ (i.e., above the bifurcation point) and correspond to the monopole excitation mode considered in Ref. [3]. They describe an elliptic fixed point, which is stable. Furthermore, we can also give the eigenvalues of the collectively excited state

$$\lambda_{-}^{(\mathrm{var})} = \pm\frac{16}{9\pi}\frac{\sqrt[4]{1+\frac{8a}{3\pi}}}{\left(\sqrt{1+\frac{8a}{3\pi}}-1\right)^2}, \tag{18}$$

which are always real for negative scattering lengths $a > -3\pi/8$, and one eigenvalue is positive. Hence, the eigenstate is unstable and belongs to a hyperbolic fixed point.

B. Stability of the numerically exact solutions

Numerically exact stationary eigenstates of the Gross-Pitaevskii Eq. (1) which are the counterpart of the variational solutions described above have been calculated in Refs. [12,13]. Here, we investigate the stability of these states and compare the results with the eigenvalues (17) and (18). For the stability analysis, we extend the procedure applied by Huepe *et al.* [22] for condensates without $1/r$ interaction in a harmonic trap to the scaled integrodifferential Eq. (3). The extended Gross-Pitaevskii equation is linearized with the Fréchet derivative, once the wave function has been decomposed in its real $\psi^R(\boldsymbol{r},t)$ and imaginary $\psi^I(\boldsymbol{r},t)$ part. The derivative is evaluated at the real-valued stationary states $\hat{\psi}_{\pm}(\boldsymbol{r})$ found in Ref. [12], which leads to two coupled equations, viz.

$$\frac{\partial}{\partial t}\delta\psi^R = \left(-\Delta-\varepsilon+8\pi a\hat{\psi}_{\pm}(\boldsymbol{r})^2-2\int d\boldsymbol{r}'\frac{\hat{\psi}_{\pm}(\boldsymbol{r}')^2}{|\boldsymbol{r}-\boldsymbol{r}'|}\right)\delta\psi^I(\boldsymbol{r},t), \tag{19a}$$

$$\frac{\partial}{\partial t}\delta\psi^I = \left(-\Delta-\varepsilon+24\pi a\hat{\psi}_{\pm}(\boldsymbol{r})^2-2\int d^3\boldsymbol{r}'\frac{\hat{\psi}_{\pm}(\boldsymbol{r}')^2}{|\boldsymbol{r}-\boldsymbol{r}'|}\right)\delta\psi^R(\boldsymbol{r},t) + 4\hat{\psi}_{\pm}(\boldsymbol{r})\int d^3\boldsymbol{r}'\frac{\hat{\psi}_{\pm}(\boldsymbol{r}')\,\delta\psi^R(\boldsymbol{r}',t)}{|\boldsymbol{r}-\boldsymbol{r}'|}. \tag{19b}$$

For the calculation of the eigenmodes we take the perturbations in the form $\delta\psi^R(\boldsymbol{r},t) = \delta\psi_0^R(\boldsymbol{r})e^{\lambda^{(\mathrm{num})}t}$ and $\delta\psi^I(\boldsymbol{r},t) = \delta\psi_0^I(\boldsymbol{r})e^{\lambda^{(\mathrm{num})}t}$. Note that $\delta\psi_0^R(\boldsymbol{r})$ and $\delta\psi_0^I(\boldsymbol{r})$ are not always real-valued. As solutions of the linearized Eqs. (19a) and (19b) they can become complex wave functions.

The numerical solution of the linearized wave equations is done with the method described in Ref. [13]. Using the "linearized potential"

$$U_1(\boldsymbol{r}) = 4\int d^3\boldsymbol{r}'\frac{\hat{\psi}_{\pm}(\boldsymbol{r}')\,\delta\psi^R(\boldsymbol{r}',t)}{|\boldsymbol{r}-\boldsymbol{r}'|}, \tag{20}$$

we can transform Eq. (19a) and (19b) into a system of three second order ordinary differential equations, which can be solved together with the stationary extended Gross-Pitaevskii equation. In order to be in a position to compare with the results of the variational approach we assume radially symmetric wave functions. The ordinary differential equations, which have to be solved, then read

$$\lambda\,\delta\psi_0^R(r)'' = -\delta\psi_0^I(r) - \frac{2}{r}\delta\psi_0^I(r)' + [8\pi a\hat{\psi}_{\pm}(r)^2 - U(r)]\delta\psi_0^I(r), \tag{21a}$$

$$\lambda\,\delta\psi_0^I(r) = -\delta\psi_0^R(r)'' - \frac{2}{r}\delta\psi_0^R(r)' + [24\pi a\hat{\psi}_{\pm}(r)^2 - U(r)]\delta\psi_0^R(r) - U_1(r)\hat{\psi}_{\pm}(r), \tag{21b}$$

$$U_1(r)'' = -\frac{2}{r}U_1(r)' - 16\pi\hat{\psi}_{\pm}(\boldsymbol{r})\,\delta\psi^R(\boldsymbol{r},t). \tag{21c}$$

The wave functions $\delta\psi_0^R(r)$ and $\delta\psi_0^I(r)$ are only determined up to a complex (normalization) constant, which they have in common. Therefore, only two real variables are required to set the initial value $[\delta\psi_0^R(0), \delta\psi_0^I(0)] = [\cos\alpha, \sin\alpha e^{i\beta}]$ for the integration. The real angles α and β, the complex eigenvalue λ, and the complex initial value $U_1^{(0)} = U_1(0)$ are the parameters which have to be searched to find the solutions of the system (21a)–(21c). The initial conditions for the first derivatives are $(\delta\psi^R)' = (\delta\psi^I)' = U_1' = 0$. The correct solutions are found when we obtain square integrable wave functions and the value of $U_1^{(0)}$ initially assumed is identical to the integral

$$U_1(0) = 16\pi\int_0^{\infty} dr'r'\hat{\psi}_{\pm}(r')\,\delta\psi_0^R(r'), \tag{22}$$

which can be calculated once the numerical wave function has been determined.

As the Gross-Pitaevskii equation is a nonlinear differential equation the correct normalization of the numerical wave functions cannot be obtained by a multiplication with a normalization constant but is possible by exploiting scaling properties of Eqs. (21a)–(21c). In the form presented here, the proper normalization and scaling of the extended Gross-Pitaevskii system is achieved by the scaling factor

$$1/\nu = \|\psi\|^2 = 4\pi\int_0^{\infty} dr|\psi(r)|^2r^2 \tag{23}$$

and the transformation of all of the following values (see Ref. [13]):

$$(\psi, r, \varepsilon, t, a, U) \to \left(\nu^2\psi, \frac{r}{\nu}, \nu^2\varepsilon, \frac{t}{\nu^2}, \frac{a}{\nu^2}, \nu^2U\right). \tag{24}$$

As can be seen from the system (21a)–(21c), the differential equations are invariant if in addition to the transformations

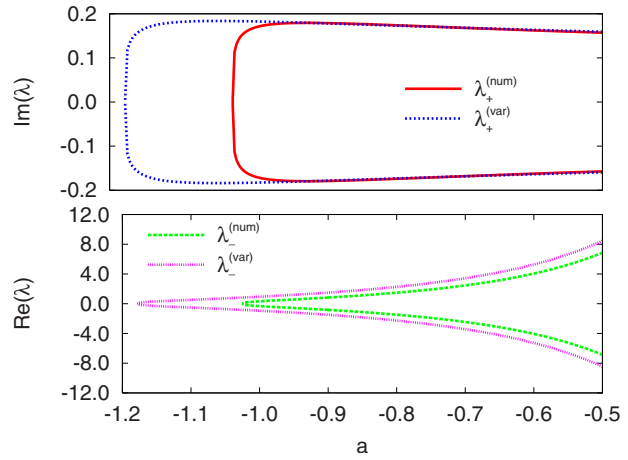

FIG. 2. (Color online) Eigenvalues of the linearization of the extended Gross-Pitaevskii system (3) for the two stationary solutions emerging at the tangent bifurcation. Both the variational (var) and the numerically exact (num) solutions are shown. The two eigenvalues λ_+ of the stationary ground state (cf. Ref. [3]) are purely imaginary demonstrating that the state is an elliptic fixed point. In contrast to this finding, the two eigenvalues λ_- of the nodeless excited state are purely real. One is positive, the other is negative. The state is an hyperbolic fixed point. Vanishing real or imaginary parts are not shown.

(24) the eigenvalue is scaled by $\lambda \to \nu^2\lambda$. Thus, it is possible to solve the system of differential Eqs. (21a)–(21c) with the unscaled and non-normalized stationary solutions $\hat{\psi}_\pm(r)$ of the nonlinear extended Gross-Pitaevskii equation computed numerically if a subsequent scaling of the eigenvalues is performed.

When the solution of the linearized system is carried out for the stationary ground state, a pair $\lambda_1=-\lambda_2$ of purely imaginary eigenvalues are found. These are plotted as a function of the scaled scattering length a in Fig. 2. The same calculation for the nodeless stationary state yields a pair of purely real eigenvalues. The qualitative agreement between the eigenvalues calculated numerically and the results obtained analytically in the variational approach is very good, but there are significant quantitative differences. Such behavior is known from previous studies of the system [12,13]. Similar to the case discussed in Ref. [22], there exist neutral modes with the eigenvalue $\lambda^{(\mathrm{num})}=0$, and additional imaginary eigenvalues are found for both stationary solutions. Altogether, the numerically exact results confirm the stability analysis performed using the analytical eigenvalues of the variational approach.

IV. DYNAMICS OF THE CONDENSATE

In this section we investigate the time evolution of arbitrary wave functions. We do this again first by the variational approach and then by exact numerical calculations. The variational calculations will reveal the different types of dynamics in the vicinity of the elliptic and the hyperbolic fixed points, viz. oscillatory or collapsing solutions. Furthermore, the collapse of the condensate for $a<a_{\mathrm{cr}}$ can be followed as a function of time. The numerically exact approach will confirm these findings and, in addition, exhibit a larger variety of qualitatively different dynamical behavior of the condensate.

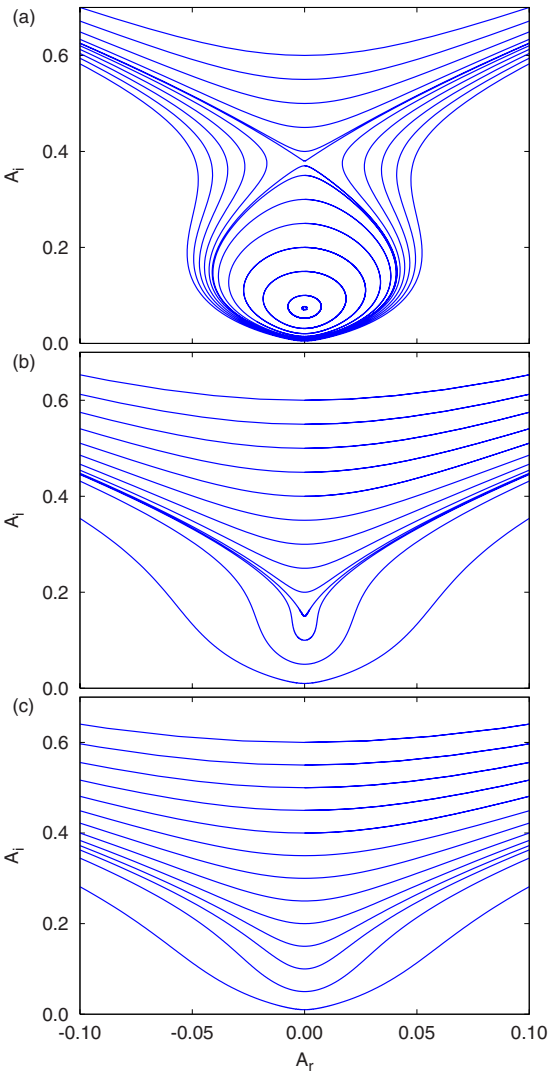

FIG. 3. (Color online) Phase portraits of the dynamics obtained from time-dependent trajectories of the complex function $A(t)$. (a) For $a=-1$ the two stationary solutions appear as fixed points. (b) They coalesce for $a=-1.18$. (c) For $a=-1.3$, below the bifurcation point, there are no stationary solutions.

A. Variational approach

We solve the two ordinary differential Eqs. (13a) and (13b) for various scaled scattering lengths a above and below the critical value $a_{\mathrm{cr}}=-3\pi/8=-1.1780$. Phase portraits of the dynamics can be obtained by plotting the imaginary part as a function of the real part of the time-dependent trajectories $A(t)=A_r(t)+iA_i(t)$. The phase portraits of trajectories with different initial conditions are shown in Fig. 3 for three values of the scaled scattering length, one above the bifurcation point [$a=-1$, Fig. 3(a)], one near the bifurcation point [$a=-1.18$, Fig. 3(b)], and one below the bifurcation point [$a=-1.3$, Fig. 3(c)]. For $a>a_{\mathrm{cr}}$ the elliptic and the hyperbolic fixed points are clearly recognizable in Fig. 3(a), they corre-

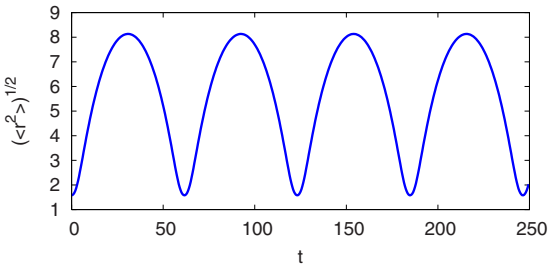

FIG. 4. (Color online) Periodically oscillating condensate for the scattering length $a=-1$ and the initial condition $A_i(0)=0.3$.

spond to the stationary eigenstates. The two fixed points coalesce at the critical scattering length a_{cr} [see Fig. 3(b)], and disappear for $a<a_{cr}$ [Fig. 3(c)] implying that no longer stationary eigenstates exist.

For the physical interpretation of the phase portraits it is useful to note that the width $\sqrt{\langle r^2\rangle(t)}$ of the condensate is related to $A_i(t)$ via

$$\langle r^2\rangle(t) = \frac{\langle\psi|r^2|\psi\rangle}{\langle\psi|\psi\rangle} = \frac{3}{4A_i(t)}. \tag{25}$$

Thus, in the stable region surrounding the elliptic fixed point the width of the condensate oscillates periodically. This is illustrated in Fig. 4 for a condensate with scattering length $a=-1$ and initial condition $A_i(0)=0.3$.

In the unstable regions $A_i(t)$ increases to infinity, which means the collapse of the condensate. In Fig. 5(a) the width $\sqrt{\langle r^2\rangle}$ is shown for a condensate with scaled scattering length $a=-1$ and initial condition close to the hyperbolic fixed point, given by Eqs. (14a) and (14b) at $A_r=0$, $A_i=0.3787$. The width first stays approximately constant, as is to be expected in the vicinity of the unstable stationary state, however, as soon as the decrease of the width becomes noticeable, the complete collapse to zero width occurs within finite time. This behavior demonstrates the existence of a collapse induced by the attractive atom-atom interactions. In a realistic experimental situation further mechanisms, which go beyond the scope of this paper, have to be taken into account. In particular, the contraction of the wave function amplifies density-dependent inelastic collisions which result in a loss of particles [23,24] and change the time evolution. Note that the calculations presented here assume a constant scaled scattering length [cf. Eq. (2)]. Of course, for initial conditions close to the hyperbolic fixed point the evolution of the collapse depends sensitively on the initial deviation from the fixed point, i.e., the closer the initial conditions approach the hyperbolic fixed point the longer it takes before the collapse sets in.

At scattering lengths $a<a_{cr}$ the square root in Eq. (14a) and (14b) becomes imaginary which means that no fixed points and thus no stationary states can exist. The condensate collapses for all initial conditions $A(0)$ of the wave function. This is illustrated for $a=-1.3$ in Fig. 5(b) with the initial condition of the "least" unstable nonstationary state $A_i(0)=\frac{1}{6a}+\frac{\pi}{8a^2}=0.10416$ [cf. Eq. (14b)]. Contrary to the situation shown in Fig. 5(a) the decrease of the condensate width starts immediately without any plateau. Ignoring a loss of

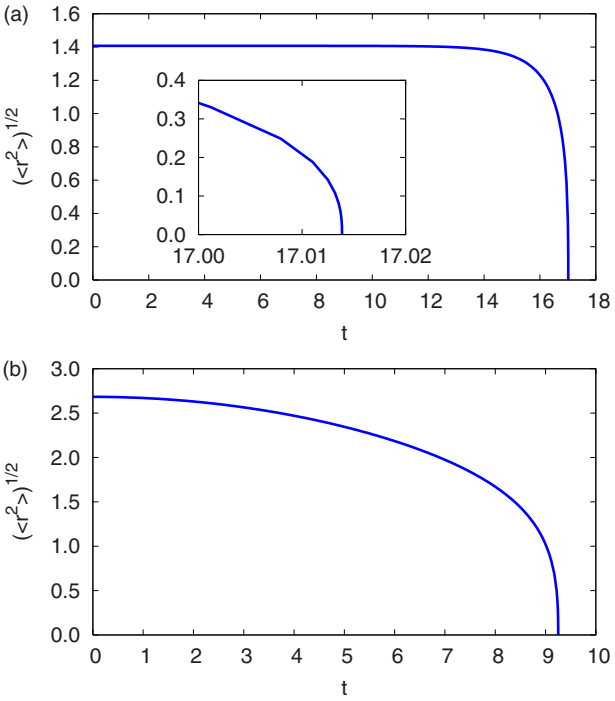

FIG. 5. (Color online) Collapse of the unstable eigenstate. (a) Scaled scattering length $a=-1$ and initial condition close to the hyperbolic fixed point at $A_r=0$, $A_i=0.3787$. The collapse after finite time is clearly visible in the inset, but depends sensitively on the initial conditions (see text). (b) Collapse of the nonstationary state at $a=-1.3$ with initial condition $A_i(0)=\frac{1}{6a}+\frac{\pi}{8a^2}=0.10416$.

particles we find that the width vanishes after the finite time $T_c=9.2522$.

The variational approach with complex parameters $A(t)$ and $\gamma(t)$ in Eq. (7) ensures that the mean-field energy

$$E = \frac{3(A_i^2+A_r^2)}{A_i} + \frac{2\sqrt{A_i}(2aA_i-1)}{\sqrt{\pi}} \tag{26}$$

is conserved. Thus, the phase portraits in Fig. 3 can be calculated alternatively as equipotential lines $E=$const instead of integrating the equations of motion (13a)–(13c).

In fact, the equations of motion obtained from the time-dependent variational principle can be brought into Hamiltonian form if the variational parameters A_r, A_i are replaced with two other dynamical quantities, of which one is assigned to be the momentum and the other the coordinate variable. Such adequate canonical variables are [25]

$$q = \frac{1}{2}\sqrt{\frac{3}{A_i}} = \sqrt{\langle r^2\rangle}, \tag{27a}$$

$$p = A_r\sqrt{\frac{3}{A_i}}, \tag{27b}$$

and in this set the mean-field energy reads

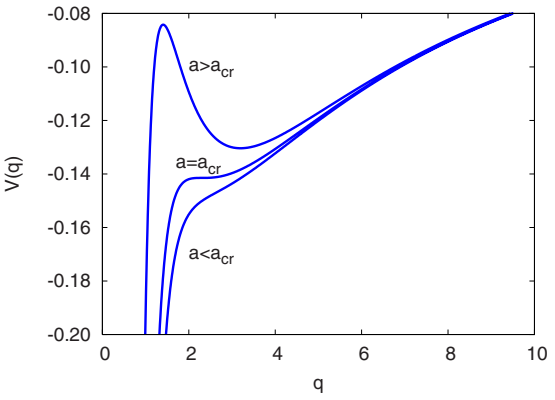

FIG. 6. (Color online) "Potential" part of the mean-field energy for different scattering lengths. This potential part of the mean field energy (28) agrees with the complete mean-field energy for stationary states of Ref. [1] (see text). The motion of the Gaussian wave function is interpreted as the one-dimensional motion of a classical particle in the potential $V(q)$.

$$E = H(q,p) = T + V = p^2 + \frac{9}{4q^2} + \frac{3\sqrt{3}a}{2\sqrt{\pi}q^3} - \frac{\sqrt{3}}{\sqrt{\pi}q} \tag{28}$$

with the decomposition into a "kinetic" part T depending on the "momentum" p and a "potential" part V depending only on the "coordinate" q. Note that q has the physical meaning of the square root of the radius of the condensate, according to Eq. (25). If the mean-field energy (28) is identified with a Hamiltonian, it describes the one-dimensional motion of a particle in the potential $V(q)$ obeying Hamilton's equations

$$\dot{q} = \frac{\partial H}{\partial p} = 2p, \tag{29a}$$

$$\dot{p} = -\frac{\partial H}{\partial q} = \frac{9}{2q^3} + \sqrt{\frac{3}{\pi}}\frac{9a}{2q^4} - \sqrt{\frac{3}{\pi}}\frac{1}{q^2}. \tag{29b}$$

Of course the backward substitution $A_r = \frac{p}{2q}$, $A_i = \frac{3}{4q^2}$ together with Eqs. (29a) and (29b) yields the same equations of motion for A_r and A_i as obtained from the TDVP. Conversely, if the trial wave function (7) had been parametrized by q, p, γ, the TDVP would have yielded their equations of motion (29a) and (29b).

The "potential" part $V(q)$ of the mean-field energy (28) is plotted in Fig. 6 as a function of the "position" variable q for different scattering lengths below, at, and above the critical scattering length a_{cr}. It agrees with the mean-field energy plotted in Ref. [1], calculated using a real-valued spherically symmetric (stationary) Gaussian trial wave function. In our approach the "kinetic" term p^2 in Eq. (28) appears additionally in the mean-field energy because of the complex ansatz (7). In other words, the full mean-field energy of Ref. [1] corresponds to our potential part V, in which the condensate moves similar to a classical particle.

Above a_{cr} the potential possesses two stationary points, a stable one at the minimum and an unstable one at the maximum. At a_{cr} the bifurcation takes place, i.e., the two extrema coincide and there is only a saddle point of the potential. For $a < a_{cr}$ the potential has no stationary points.

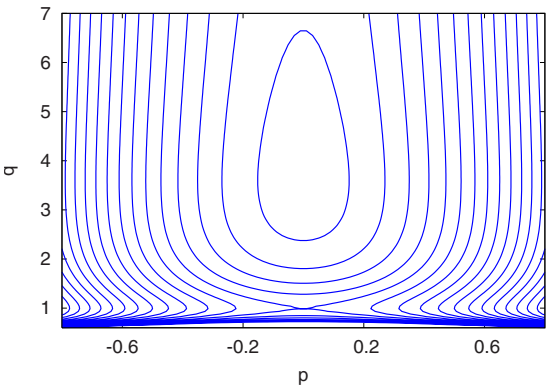

FIG. 7. (Color online) Phase portrait of the mean-field energy formulated in the canonical variables q and p for $a=-0.8$.

For $a > a_{cr}$ the motion of the condensate is stable as long as the mean-field energy lies below the maximum of the peak of the potential and if it is located close to the local minimum on the right-hand side of the unstable fixed point. The one-dimensional motion is periodic between two turning points. If the energy is increased above the energy of the unstable fixed point, only one turning point remains, and the condensate collapses when q approaches zero.

Expanding the potential about the minimum and maximum leads to the frequencies (17) of oscillations of the ground state and the decay rates (18) of the collectively excited state. The phase space portrait of the dynamics in (p,q) variables is presented in Fig. 7 for the scattering length $a=-0.8$. The equipotential lines which asymptotically approach the $q=0$ axis represent the collapse of the condensate.

B. Exact time-dependent calculations with the split-operator method

The split-operator method [26] assumes the decomposition of the Hamiltonian $H=T+V$, and makes use of the short-time approximation for the time evolution operator

$$e^{-i\tau(T+V)} = e^{-i(\tau/2)T}e^{-i\tau V}e^{-i(\tau/2)T} + O(\tau^3). \tag{30}$$

The kinetic part of the evolution operator is applied to the wave function in momentum space, the potential part is applied to the wave function in position space representation. The method is numerically especially efficient when a fast Fourier transform is used for the transition from momentum to position space representation and backward. For the nonlinear Gross-Pitaevskii Eq. (3) the potential part of the time evolution operator needs some further investigation in comparison with the linear Schrödinger equation. Although the scattering term V_c belongs to the nonlinear part of the Gross-Pitaevskii equation, it can be treated as a conventional potential of a linear Schrödinger equation and presents no additional difficulty. The $1/r$ interaction potential V_u, however, requires the additional solution of the integral (4b) after every time step of integration. This integral is computed using the convolution theorem, i.e.,

$$\mathcal{F}\{V_u(r,t)\} = \mathcal{F}\left\{\frac{1}{r}\right\}\mathcal{F}\{|\psi(r,t)|^2\}, \tag{31}$$

where the Fourier transform of $1/r$ is performed analytically to give

$$\mathcal{F}\left\{\frac{1}{r}\right\} = \frac{4\pi}{p^2}. \tag{32}$$

Altogether two additional fast Fourier transforms are necessary per time step and we obtain for the $1/r$ interaction term

$$V_u(r,t) = -\frac{16}{r}\int_0^\infty dp \frac{\sin pr}{p^2}\int_0^\infty dr' r'|\psi(r',t)|^2 \sin pr'. \tag{33}$$

The fast Fourier transforms are performed on equidistant grids with 1024 or 2048 points. The numerical convergence is checked by monitoring that the wave function vanishes at the $r_{\max}$, $p_{\max}$ border of the grid in position as well as in momentum space. Due to the widening of the wave function in some computations the necessary size of the grid depends on the desired propagation time. A criterion of convergence for the time step of the split-operator method is that the mean-field energy is a constant of motion. In particular for the computations in which the wave function is very close to the hyperbolic fixed point the time step must be chosen small for convergence. Specifically, for the computations in the vicinity of the hyperbolic fixed point we use $\Delta t = 0.0001$ whereas for computations far away from the unstable stationary state a time step of $\Delta t = 0.01$ is sufficient.

In the following paragraphs, the dynamics of the condensate is investigated for regions initially close to the two stationary states. In particular, we present the evolution of those initial states which are obtained by deforming the stable and the unstable stationary state by

$$\psi \to \psi f, \quad r \to r/f^{2/3} \tag{34}$$

with a stretching factor f, i.e., for $f=1$ the stable and the unstable stationary state, respectively, are obtained. This choice of perturbation leaves the norm of the wave function unchanged.

We start with the investigation of the dynamics of wave functions close to the unstable stationary state. In Fig. 8(a) the square root of the width (25) of the condensate is plotted as a function of time. The evolution presented in Fig. 8(a) is computed at the scaled negative scattering length $a=-0.85$ with a deformation factor $f=1.001$. The wave function itself is plotted in Fig. 8(b) as a function of the radial coordinate r at different times. The initial wave function is given by the solid red line. The condensate stays nearly stationary at the beginning for times up to $t \approx 4$, i.e., the dashed green line in Fig. 8(b) representing the wave function at $t=4$ nearly coincides with the initial state, and the width [Fig. 8(a)] has only slightly decreased from $\sqrt{\langle r^2\rangle}=1.48$ at $t=0$ to $\sqrt{\langle r^2\rangle}=1.44$ at $t=4.0$.

With increasing time and the farther away the wave function has moved from the stationary state, the shrinking of the width of the wave function is accelerated. As already predicted by the variational computation this leads to a collapse

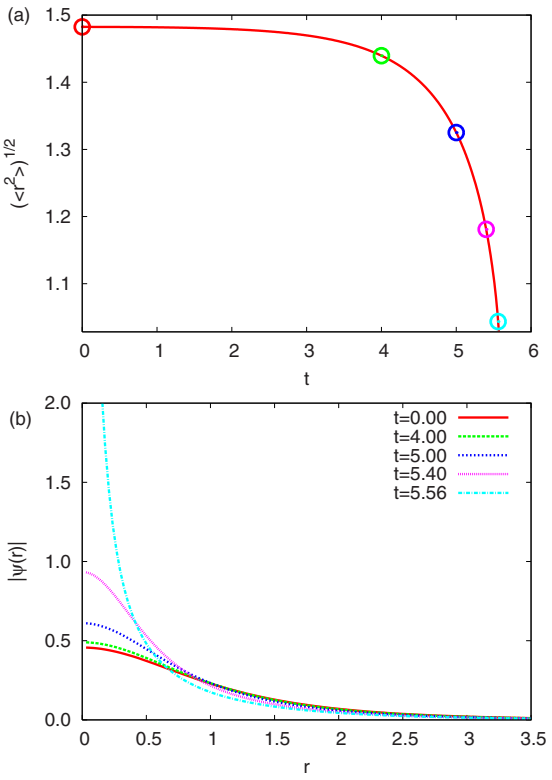

FIG. 8. (Color online) (a) Width of a slightly perturbed stationary state ($a=-0.85$, $f=1.001$) as a function of time. (b) Wave functions of the state for selected times marked by circles in (a). The collapse of the condensate is obvious from both plots.

of the condensate at finite time. Both Figs. 8(a) and 8(b) show that the width of the condensate tends to zero in position space when the collapse time T_c is approached. Conversely, in momentum space the wave function becomes arbitrarily wide close to T_c. Thus, the size of the grid in momentum space is the numerically limiting factor for the propagation with the split-operator method. Choosing a large grid in momentum space allows for integrating arbitrarily close to T_c.

According to the variational results there exist periodic solutions in the vicinity of the unstable stationary state, and, indeed, similar behavior is found in the numerically exact computations. In Fig. 9(a) the width of a quasiperiodically oscillating condensate at $a=-1.0$ is shown. The associated wave function is plotted in Fig. 9(b) for different times.

It can be seen that at the times where the root-mean-square extension of the condensate goes through a maximum, or minimum, there is also a good agreement of the respective wave functions. This shows that the wave functions indeed oscillate quasiperiodically. The calculation is started with the wave function of the unstable stationary state ($f=1$). Because of numerical deviations, the solution begins to oscillate for times larger than $t \approx 25$. In contrast to the variational result, the oscillation of the condensate is not strictly periodic here.

The dynamics of the condensate presented so far does not qualitatively differ from what is predicted by the variational calculation. In Fig. 10(a), however, the situation is encountered where the width increases monotonically with time.

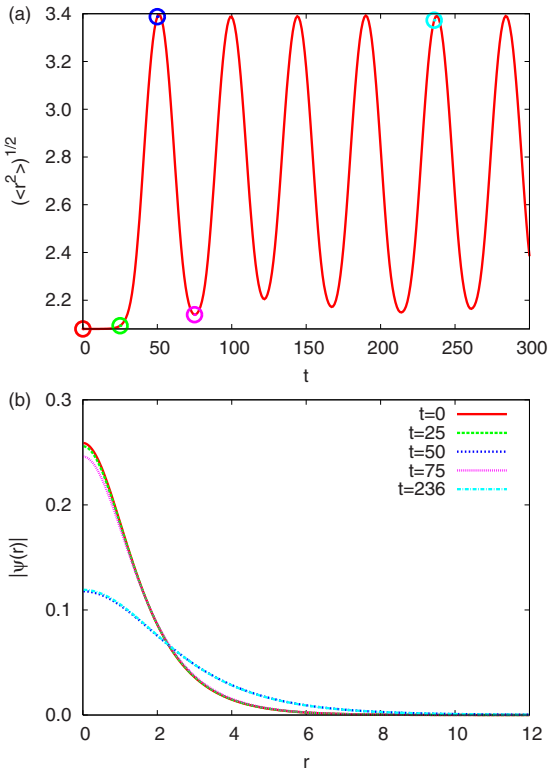

FIG. 9. (Color online) Evolution of the unstable "stationary" state ($f=1$) at $a=-1.0$. (a) Due to numerical deviations an oscillation of the width starts for times larger than $t\approx 25$. (b) Corresponding wave functions for the times marked in (a).

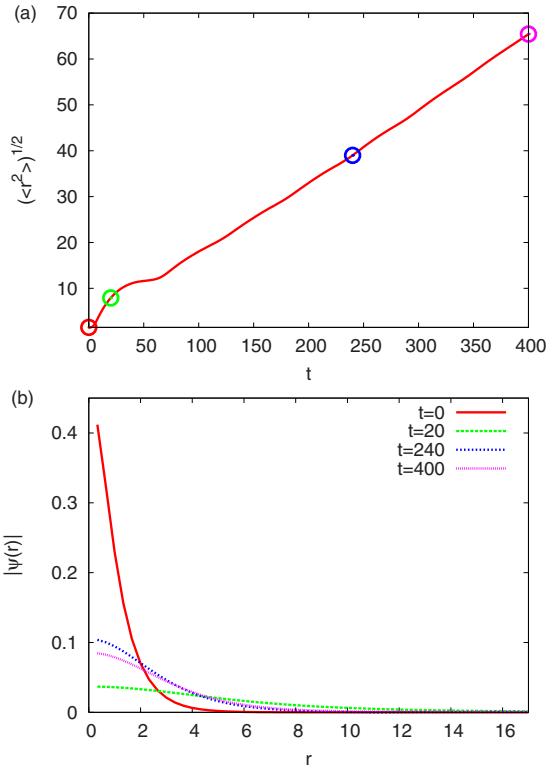

FIG. 10. (Color online) (a) The width of the condensate, initially in the vicinity of the unstable fixed point with $f=0.99$ and $a=-0.85$ increases linearly with time for $t\gtrsim 65$. (b) Wave functions of the same state for different times marked by circles in (a). The wave functions at $t=240$ and $t=400$ seem to be sharper than the wave function at $t=20$. Note that a larger step size on the grid in position space than in Figs. 8 and 9 was used. Therefore there is a visible distance between $r=0$ and the first point on the grid.

Here we have chosen a deformation of $f=0.99$ at the scaled scattering length $a=-0.85$. For short times there is again a plateau where the width is nearly constant as in Fig. 9(a). The plateau is shorter than that in Fig. 9(a) because the initial wave function of Fig. 10(b) differs more from the stationary state than the initial state associated with Fig. 9(a). For times $t\gtrsim 65$, however, the width increases linearly with time. Obviously Fig. 10(b) shows a broadening of the wave function for times up to $t\approx 20$. For longer times the main peak of the wave function located at the origin does not broaden monotonically with time as might be concluded from Fig. 10(a). Indeed, the wave functions at $t=240$ and $t=400$ seem to be even sharper than the wave function at $t=20$ in Fig. 10(b). This apparent contradiction is resolved, if the wave functions are plotted on a broader range in position space and on a logarithmic scale, which is presented in Fig. 11. Here it is clearly visible that the wave functions have more than one peak and their width does increase for larger times. However, the amplitude of the run-away parts is very small compared to the first maximum at the origin. For obtaining the accurate propagation it is therefore necessary to choose a large grid in position space to make the wave function vanish on the border, in particular for long propagation times. The usual method to prevent the wave function from running to the border of the grid and being reflected there, namely, to introduce an absorbing complex potential, is not applicable for the nonlinear Gross-Pitaevskii system, in which an absorption of the wave function alters the potential.

In the vicinity of the stable stationary state the condensate exhibits an oscillatory behavior shown in Fig. 12(a). The parameter values for this computation are a stretching of $f=1.01$ of the stable stationary state at $a=-0.85$. The amplitude of the oscillation is very small compared to the oscillation in Fig. 9(b) and ranges from about $\sqrt{\langle r^2\rangle}=3.336$ to

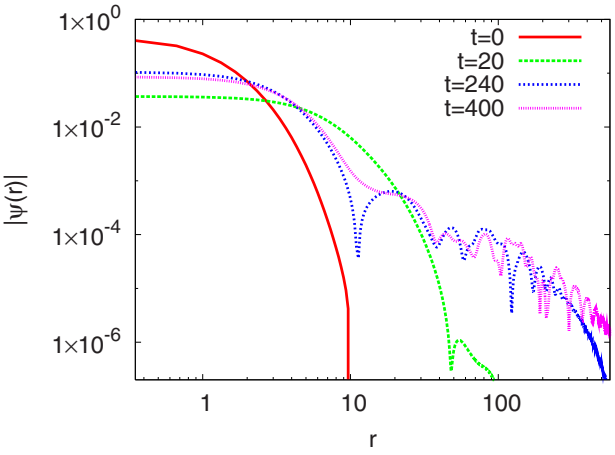

FIG. 11. (Color online) Double logarithmic plot of the wave functions presented in Fig. 10(b). The long range tail occurring with increasing propagation times and leading to a monotonically increasing width in Fig. 10(a) becomes visible.

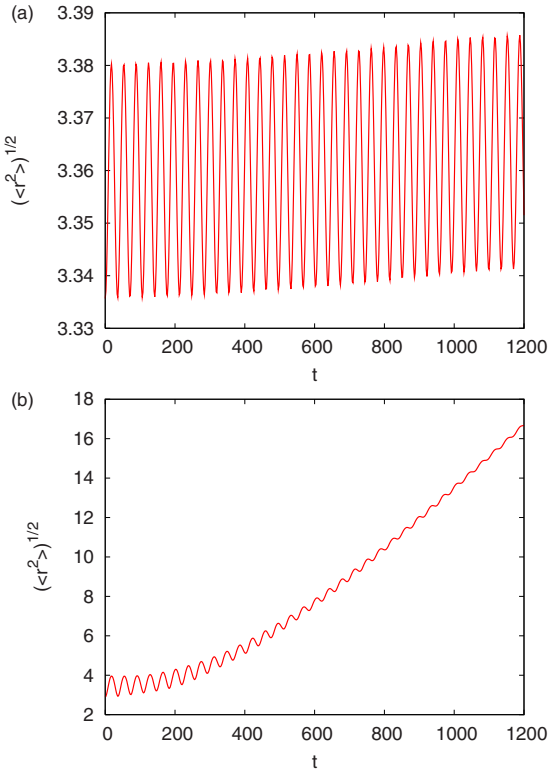

FIG. 12. (Color online) (a) Quasiperiodically oscillating condensate at a scaled scattering length of $a=-0.85$ and $f=1.01$. (b) An initially quasi periodically oscillating condensate at $a=-0.85$, $f=1.25$ turns into expanding dynamics after long time.

$\sqrt{\langle r^2\rangle}=3.385$. This observation is in correspondence with the variational result in Fig. 3(a) where small deviations from the stable fixed point lead to small oscillations around the fixed point along the equipotential lines whereas small deviations from the unstable fixed point may lead to oscillations with a large amplitude. However, with increasing distance from the stable fixed point the dynamics is no longer oscillatory, but, as can be seen in Fig. 12(b), there is also a gradual broadening of the condensate, which becomes more pronounced for larger deviations of the initial wave function from the stable stationary state as is shown in Fig. 12(b), in which the time evolution of the width for $f=1.25$ is plotted. The scattering length is set to $a=-0.85$ again. Here, the oscillatory motion at the beginning changes to a mainly expanding motion with minor modulations.

V. CONCLUSION

We have investigated the time-dependent extended Gross-Pitaevskii equation for self-bound Bose-Einstein condensates with attractive $1/r$ interaction. The two stationary states of the system, which emerge in a tangent bifurcation, and were found with time-independent calculations in Refs. [1,12], were identified as an elliptic and a hyperbolic fixed point of the dynamical system. A time-dependent variational approach opened the possibility to obtain analytical results for the eigenvalues of the linearized equations of motion, which is a feature of the self-trapped condensate with $1/r$ interaction. Numerically exact calculations confirmed the variational findings.

The dynamics of the system was analyzed with the time-dependent variational approach and numerically exact computations with the split-operator method. For scaled scattering lengths larger than the critical value an oscillatory behavior of the condensate was found in the vicinity of the stationary solutions. It was shown that it is possible to introduce canonical variables and interpret the dynamics of the width of the condensate as the motion of a classical particle in a potential. Furthermore, there are unstable regions of the phase space, in which a collapse of the condensate occurs. For scaled scattering lengths below the critical value the condensate is always collapsing. The numerically exact method revealed solutions with a continuously expanding motion of the width.

The self-bound spherically symmetric Bose-Einstein condensates with gravitylike interaction investigated in this paper are unique in so far as variational calculations to a large extent can be performed analytically. The results obtained in this way can serve as a useful guide to numerical calculations, and to the exploration of the nonlinear dynamic properties of more general Bose-Einstein systems. The appearance of stable elliptic islands, with elliptic fixed points, unstable regions, with hyperbolic fixed points, and of separatrices dividing the regions, are typical signatures of autonomous Hamiltonian systems. Therefore they will also be present if a symmetric trap potential is added to the contact and gravitylike interaction.

In anisotropic condensates the variational approach will lead to autonomous Hamiltonian dynamics with more than one degree of freedom. Therefore in addition to the signatures discussed in this paper signatures of chaos can appear. In fact, a recent variational investigation of Bose-Einstein condensates with a dipole-dipole interaction [27] has revealed that, as the mean-field energy is increased from its ground-state value, chaotic regions emerge in phase space which coexist with regular islands, corresponding to irregularly fluctuating or quasiperiodically oscillating states of the condensates, respectively. The investigations presented in this paper have paved the way for studies of this sort in realistic Bose-Einstein condensates with long-range interactions.

ACKNOWLEDGMENTS

This work was supported by Deutsche Forschungsgemeinschaft. H.C. is grateful for support from the Landesgraduiertenförderung of the Land Baden-Württemberg.

[1] D. O'Dell, S. Giovanazzi, G. Kurizki, and V. M. Akulin, Phys. Rev. Lett. **84**, 5687 (2000).
[2] S. Giovanazzi, D. O'Dell, and G. Kurizki, Phys. Rev. A **63**, 031603(R) (2001).
[3] S. Giovanazzi, G. Kurizki, I. E. Mazets, and S. Stringari, Europhys. Lett. **56**, 1 (2001).
[4] L. Santos, G. V. Shlyapnikov, P. Zoller, and M. Lewenstein, Phys. Rev. Lett. **85**, 1791 (2000).
[5] M. Baranov, L. Dobrek, K. Góral, L. Santos, and M. Lewenstein, Phys. Scr. **T102**, 74 (2002).
[6] K. Góral, L. Santos, and M. Lewenstein, Phys. Rev. Lett. **88**, 170406 (2002).
[7] K. Góral and L. Santos, Phys. Rev. A **66**, 023613 (2002).
[8] S. Giovanazzi, A. Görlitz, and T. Pfau, J. Opt. B: Quantum Semiclassical Opt. **5**, S208 (2003).
[9] A. Griesmaier, J. Werner, S. Hensler, J. Stuhler, and T. Pfau, Phys. Rev. Lett. **94**, 160401 (2005).
[10] J. Stuhler, A. Griesmaier, T. Koch, M. Fattori, T. Pfau, S. Giovanazzi, P. Pedri, and L. Santos, Phys. Rev. Lett. **95**, 150406 (2005).
[11] T. Koch, T. Lahaye, J. Metz, B. Fröhlich, A. Griesmaier, and T. Pfau, Nat. Phys. **4**, 218 (2008).
[12] I. Papadopoulos, P. Wagner, G. Wunner, and J. Main, Phys. Rev. A **76**, 053604 (2007).
[13] H. Cartarius, J. Main, and G. Wunner, Phys. Rev. A **77**, 013618 (2008).
[14] T. Kato, *Perturbation Theory for Linear Operators* (Springer, Berlin, 1966).
[15] W. D. Heiss, Eur. Phys. J. D **7**, 1 (1999).
[16] W. D. Heiss, J. Phys. A **37**, 2455 (2004).
[17] U. Günther, I. Rotter, and B. F. Samsonov, J. Phys. A **40**, 8815 (2007).
[18] H. Cartarius, J. Main, and G. Wunner, Phys. Rev. Lett. **99**, 173003 (2007).
[19] P. A. M. Dirac, Proc. Cambridge Philos. Soc. **26**, 376 (1930).
[20] A. D. McLachlan, Mol. Phys. **8**, 39 (1964).
[21] V. M. Pérez-García, H. Michinel, J. I. Cirac, M. Lewenstein, and P. Zoller, Phys. Rev. A **56**, 1424 (1997).
[22] C. Huepe, L. S. Tuckerman, S. Métens, and M. E. Brachet, Phys. Rev. A **68**, 023609 (2003).
[23] Y. Kagan, A. E. Muryshev, and G. V. Shlyapnikov, Phys. Rev. Lett. **81**, 933 (1998).
[24] E. A. Donley, N. R. Claussen, S. L. Cornish, J. L. Roberts, E. A. Cornell, and C. E. Wieman, Nature (London) **412**, 295 (2001).
[25] J. Broeckhove, L. Lathouwers, and P. V. Leuven, J. Phys. A **22**, 4395 (1989).
[26] M. D. Feit, J. A. Fleck, Jr., and A. Steiger, J. Comput. Phys. **47**, 412 (1982).
[27] Köberle, H. Cartarius, T. Fabčič, J. Main, and G. Wunner, e-print arXiv:0802.4055.